Chem Biol Drug Des 2012; **80:** 561–571

Research Article

doi: 10.1111/j.1747-0285.2012.01429.x

Molecular Dynamics Simulations of Peptide Inhibitors Complexed With *Trypanosoma cruzi* Trypanothione Reductase

Samuel Silva Da Rocha Pita[1,*,†], Paulo Ricardo Batista[1], Magaly Girão Albuquerque[2] and Pedro Geraldo Pascutti[1]

[1]*Instituto de Biofísica Carlos Chagas Filho, Universidade Federal do Rio de Janeiro, Avenida Carlos Chagas Filho, 373, Bloco D, Sala D-030, Cidade Universitária, Ilha do Fundão, 21941-902 Rio de Janeiro, RJ, Brasil*

[2]*Instituto de Química, Universidade Federal do Rio de Janeiro, Rio de Janeiro, RJ, Brasil*

**Corresponding author: Samuel Silva Da Rocha Pita, samuelpita@biof.ufrj.br*

[†]*Present address: Faculdade de Farmácia, Universidade Federal da Bahia, Rua Barão do Jeremoabo, 147, Campus de Ondina, 40.170-115 Salvador, BA, Brasil.*

The drugs against tropical neglected diseases, especially Chagas' Disease, were launched more than 30 years ago, and the development of resistance requires the discovery of new and more effective chemotherapeutic agents. *Trypanosoma cruzi* has a redox enzyme called trypanothione reductase which was successfully inhibited for peptide derivatives (McKie *et al.*, Amino Acids, 2001, 20: 145). This work aims at studying the mechanism of inhibition of this enzyme through molecular dynamics simulations and evaluating the behavior of some derivatives when inhibiting this protein. We should affirm that any particular molecular dynamics analysis tools (Hbond pattern, 3-D root-mean-square deviation, solvent accessible surface area, etc.) cannot be used apart from the others to justify completely these peptides inhibitory patterns. Based on our results, we reproduced the experimental data and, moreover, we discriminated against a new site in enzyme aperture, which can assist the development of powerful inhibitors against trypanothione reductase enzyme.

Key words: hydrogen bond, molecular dynamics simulations, neglected diseases, peptide inhibitors, trypanothione reductase

Received 13 March 2012, revised 1 May 2012 and accepted for publication 31 May 2012

Since its discovery more than a century ago (1), Chagas' disease is endemic over a region roughly the size of an area from the Great Lakes of North America (~42°N) to southern Patagonia (~46°S) (2). Besides, it has been spreading to other areas because of migration of infected people (3–8). The causative agent of Chagas' disease, *Trypanosoma cruzi* (*T. cruzi*), is a protozoan grouped together with *Leishmania* (9). Both these genera cause maladies that are classified as neglected diseases and are responsible for over half a million annual human deaths (2,4,9,10). In particular, Chagas' disease is the secondary cause of cardiomyopathy (11).

The only two drugs licensed for the treatment of Chagas' disease (nifurtimox and benznidazole) were launched in 1967 and 1972, respectively (12). These drugs are at most active in acute or short-term chronic infections, but have very low anti-parasitic activity against the prevalent chronic form of the disease (12). Owing to the substandard commercial interest from pharmaceutical companies in developing drugs for tropical illnesses, the pipeline of new drugs for these diseases has virtually dried up during the past three decades (9). To date, the public health strategy adopted for combating these diseases focused on the vector control (2,13). Even without a large investment, several new antiprotozoan drugs are under development for Chagas' disease, leishmaniasis and human African trypanosomiasis (9,14).

All trypanosomes and leishmania (*Kinetoplastida* order) posses a unique thiol metabolism, and both rely on the trypanothione [disulfide, TS_2, and thiol forms, $T(SH)_2$] and trypanothione reductase (TR) system. In 1985, TR was firstly described in *Crithidia fasciculata*, a non-human pathogen (15). The TR essential action in reducing the trypanothione disulfide (TS_2) substrate is crucial for the maintenance of a reducing intracellular milieu in the parasite (15,16). Genetic studies revealed that modifications in TR gene (disruption or *over-expression*) affect the parasite's ability to survive in oxidative stress (17–20). Therefore, the TR main role in the parasite and its absence from the mammalian host turns the enzyme an attractive target for structure-based drug design (16). In fact, many compounds were tested against TR and some of them presented specific inhibition, i.e., they did not inhibit the human counterpart, glutathione reductase [(16), and references therein].

The first actual advance in TR inhibitor design came from a rational design approach (21), which identified tricyclic antidepressant framework as selective TR lead-inhibitor (22). Pointing out that the TR enzyme acts as a dimer and peptide mimetic compounds can selectively and competitively block the monomers (23), McKie *et al.* (24) tested some peptide derivatives as specific TR inhibitors. The

most potent peptide derivative presented a concentration responsible for 50% of enzyme inhibition (IC_{50}) equals to 10.4 μM and the second one, IC_{50} = 11.8 μM (24). As peptides can provide us rapid lead information (24), the inhibitory mechanism of a subset of compounds of this class was studied against TR applying molecular dynamics (MD) simulations.

It is well known that TR depends on the flavin to catalyze its biologic reaction, specifically flavin-adenine-dinucleotide (FAD) (10,15), as some crystallographic works pointed out the importance of the flavin binding site at the enzyme (25–27). The non-covalently bound FAD cofactor is the redox prosthetic group situated near the active site, and participates in a hydride ion transfer from the dihydro-nicotinamide-adenine-dinucleotide phosphate (NADPH coenzyme) to the catalytic cysteines (Cys^{53}-Cys^{58}) (28). Therefore, each TR monomer comprises four domains, i.e., a FAD-binding domain, an NADPH-binding domain, a region composed by Cys^{53}-Cys^{58} (disulfide bond) and $His^{461'}$ (the prime character means that this residue belongs to chain B), where the catalysis occurs, and, an interface domains.

For several decades, the physical chemistry of isoalloxazine ring and the two most common flavin cofactors, flavin mononucleotide (FMN) and FAD, have been subject of investigation [see reference (29) and references cited therein], but none of the authors had yet studied these species behavior into the TR (30). Thus, the dynamic behavior of the FAD binding site into TR by MD was also analyzed.

Material and Methods

Preparing the peptide inhibitor structures

Among many structures of the *T. cruzi* TR available at the Protein Data Bank (PDB) (31), the one coded 1BZL (oxidized form) (25) was selected. This choice was based on two major points: (i) this structure is bound to the natural substrate (TS_2) and FAD cofactor; and (ii) it presents higher resolution (R = 2.40 Å) than another deposited earlier at the PDB (25,26).

All the ligand structures from the peptide series, synthesized and tested by McKie *et al.* (24) (Table 1), were built in SYBYL 7.0 package[a]. The structures were further energy minimized using Tripos force field and the conjugated gradient algorithm, until reaching a gradient of 0.05 kcal/mol. The distance dependent dielectric function (ε = 3.00) was used within a cutoff at 10 Å. Gaisteger-Hückel charges were calculated for the ligands, assuming that the ionizable groups (i.e., amine, guanidine, and carboxylic acid) were in their ionic forms at physiologic pH.

Preparing the enzyme-ligands complexes

The crystallographic structure of TR (PDB code 1BZL) has two FAD and two TS_2 molecules. To create the TR-peptide complex models, we removed the TS_2 structure from the complex, and each one of the 21 peptides (24) was docked in the TR active site using the FLEXX program (32). The pose (conformation and orientation) with the highest docking energy score was selected, according to the total FLEXX scoring function value.[a] The 21 peptides, docked by FLEXX program in our previous work (32), followed the same pattern as the reported IC_{50} values (24).

From this set of 21 peptides, a sub-set of six inhibitors, namely derivatives **10**, **9**, **16**, **8**, **13**, and **18** were renumbered here from **1** to **6**, according to increase inhibitory potency (see Figure 1 and Table 1), as they are representative of the 21 peptide derivatives synthesized at the original work (24): the most (**5** and **6**), medium (**3** and **4**), and less (**1** and **2**) active compounds and the bulkier peptide (**3**).

As the homodimeric TR enzyme overall structure will be analyzed, it was necessary to include each ligand's duplicate (TS_2 or peptide inhibitors) at the other monomer site. The second ligand was modeled applying the *Deep View* module in Swiss-PDB Viewer (33), merging both chains and translating each ligand coordinates from one site to the other.

MD parameterization

The FAD (FMN and AMP subunits) parameters were taken from the GROMOS96 force field (34,35). Bond lengths, bond angles, proper, and improper dihedral angle and other parameters for FMN and AMP *building blocks* were used as described before (29).

Table 1: Physicochemical properties of the substrate (trypanothione disulfide, TS_2) and the six peptide derivatives used in this study

#[a]	Name	pIC_{50}[b]	MV[c]	MC[d]	SASA[e]	Hbond[f]
TS_2	N^1,N^8-bis(γGlu–Cys–Gly)spermidine	n.a.	1 798	+1	0.81 ± 0.03	5.53 ± 1.18
1 (**10**)	H-His-Trp-Lys-OH	2.41	1 305	+1	0.45 ± 0.02	5.95 ± 1.66
2 (**09**)	H-His-Trp-His-OH	2.76	1 251	0	0.75 ± 0.03	5.25 ± 1.65
3 (**16**)	BZO-Gly-Arg-Arg-Leu-BNF	3.29	2 030	+2	0.63 ± 0.03	6.55 ± 1.93
4 (**08**)	BEZ-Arg-Arg-PNO	4.22	1 666	+2	1.02 ± 0.05	6.45 ± 2.17
5 (**13**)	BZO-Leu-Arg-Arg-BNF	4.93	1 912	+2	0.70 ± 0.03	11.68 ± 2.32
6 (**18**)	BEZ-Ala-Arg-Arg-4-methoxy-BNF	4.98	1 985	+2	0.62 ± 0.03	7.21 ± 1.79

BZO, benzoyl; BNF, β-naphtylamide; BEZ, benzyloxycarbonyl; PNO, *para*-nitroanilide.
[a]The number between parentheses is the corresponding derivative number according to reference (22).
[b]pIC_{50} (M), $pIC_{50} = \log(1/IC_{50})$, IC_{50} data taken from (22).
[c]The molecular volume (MV, $Å^3$) was calculated using the QSAR Properties of HyperChem™ (version 7.5).
[d]The molecular charge (MC).
[e]The solvent accessible surface area (SASA) was calculated using the DSSP program (50) inside GROMACS package (31).
[f]Hydrogen bonds (Hbond) interactions between trypanothione reductase and ligands (mean ± SD).

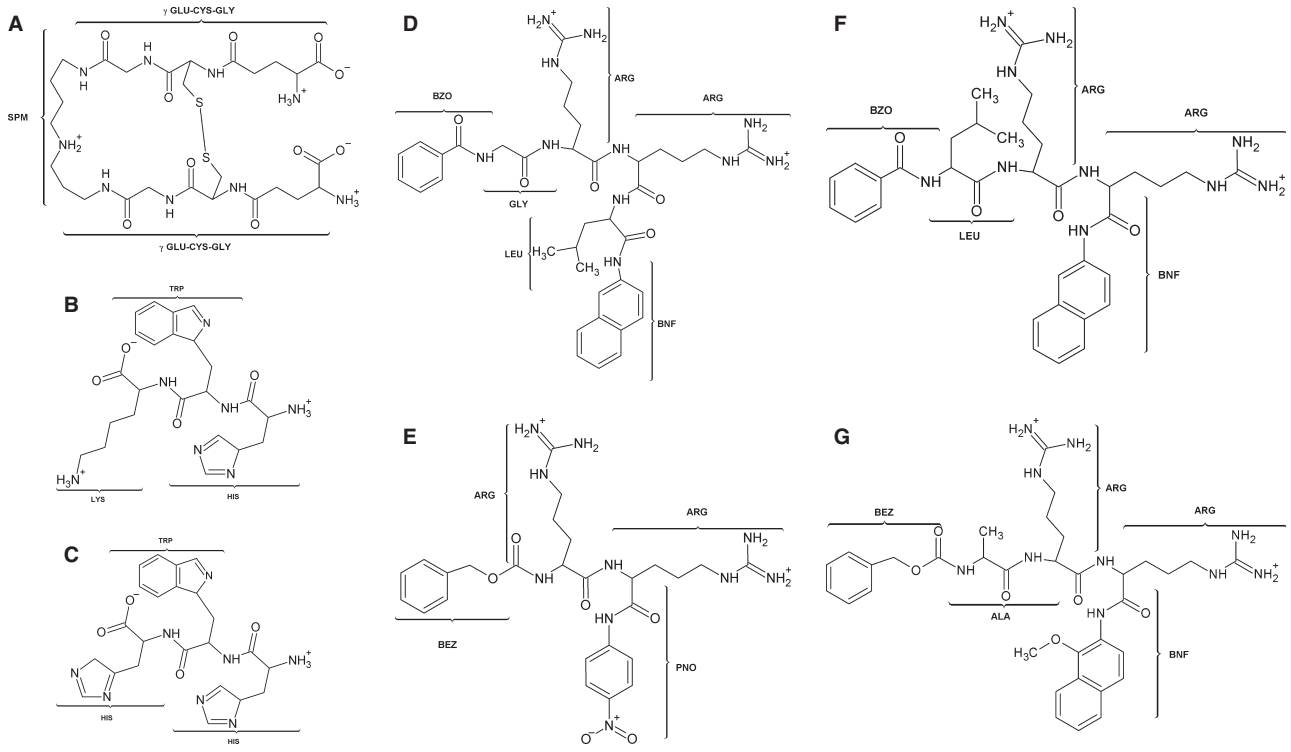

Figure 1: Chemical structures and group definitions of the compounds used in the molecular dynamics simulations complexed with *Trypanosoma cruzi* trypanothione reductase. In (A), chemical structural representation of the natural substrate trypanothione (TS2). From (B) to (G) the same representation for peptides **1**–**6** (as described at Table 1).

The same *building blocks* methodology (36) applied for FAD was used to construct the other ligands in this study. The peptide parameters were taken from the GROMOS96 force field (34,35) and the non-amino acid subunits were approached to the most similar amino acid residue. It was built for the *benzoyl* (BZO), *benzyloxy-carbonyl* (BEZ) and *para-nitroanilide* (PNO) fragments were built based on the phenylalanine parameters; *β-naphtylamide* (BNF) derivatives were based on tryptophan; and the *spermidine* (SPM) TS_2 moiety is analogous to the lysine side chain. Atomic charges, bonds, angles, dihedrals were adapted to each ligand structure. To check the validity of this approach, 10 nanoseconds of MD simulations of each ligand were performed in a simulation box with water and counter-ions.

MD settings

The systems were simulated using the GROMACS 3.3 version package (36) in a NPT ensemble. GROMOS96 force field (34,35) was used for all simulations. The water solvent, Simple Point Charge (SPC) model (37), was inserted into a dodecahedral box at a distance of 1.0 nm from the protein surface. This distance ensures that the minimum distance between the molecules and its periodic image is larger than the cutoff used for the Lennard–Jones interactions (0.9 nm). To neutralize the systems, some water molecules were replaced by positive ions (Na^+), randomly distributed inside the box. Each system has approximately 139 000 particles.

A three-step procedure (5000 steps each) of energy minimization was used to avoid artifacts in atomic trajectories, because of the conversion of potential energy into kinetic energy (34). First, a steepest-descent algorithm was applied, restraining harmonically the protein non-hydrogen atoms to their initial positions; followed by a second steepest descent minimization with all atoms unrestrained. Subsequently, a conjugated gradient algorithm was applied to the entire system for further energy minimization. The bonds involving hydrogen atoms were constrained using the LINCS (38) algorithm for protein/ligands and with SETTLE (39) for water molecules, allowing the use of a 2 femtosecond integration time. Periodic boundary conditions were applied, and the non-bonded cutoffs were set to 0.9 nm for both, the Coulomb and the van der Waals interactions. The long range electrostatic interactions were treated using the particle-mesh-Ewald method (40).

A 1 nanoseconds MD equilibration, at 298 K, was performed with the protein non-hydrogen atoms position restrained. In this step, a random Boltzmann distribution was used to generate the initial velocities for each simulation. Temperature and pressure were kept constant at 298 K and 1 atm, using the Berendsen weak-coupling approach (41). Then, 10 nanoseconds of MD with no restrictions were performed for data achievement.

Contact area between TR and ligands

The intermolecular contact surface area between TR and ligands was calculated from the MD trajectories with the 'SURFINMD' software, a program based on the Connolly algorithm (42), developed by Pascutti *et al.*, being extensively employed by our group (43–47).

From the protein and ligand solvent accessible surface area (SASA), it is possible to determine the intermolecular surface as being the intersection between the protein and ligand SASA, i.e., the sum of the areas of protein and ligand, is close enough to avoid the allocation of a water molecule used as a probe (1.4 nm).

Results and Discussions

MD simulations stability

The protein's structural thermal fluctuation is intimately coupled to its function (48), instead of only representing random events (49). Herein, are presented the results of explicit solvent MD simulations of the *T. cruzi* TR homodimeric free (*apo* form), bound to FAD (*holo* form), complexed with its natural substrate TS_2 or with each of the six peptide inhibitors (Table 1). The NADPH coenzyme was not included into the simulations because it has a transient participation in the enzyme mechanism, on a hydride ion NADPH transfer to FAD. Therefore, a total of nine TR systems was simulated, namely *apo*-TR (free TR, i.e., TR in the *apo* form), *holo*-TR (TR bound to FAD, i.e., TR in the *holo* form), TR_{TS2} (TR + FAD + TS_2), and $TR_{1–6}$ (TR + FAD + peptide **1**–**6**). First, the time evolution of the root-mean-square deviation (RMSD) of TR atoms was monitored during the simulation (Figure 2A). In other words, how the protein deviates over time from the initial structure (final protein conformation obtained after position-restrained MD) (see details in the Material and Methods section). Figure 2A shows that all the systems present a relative RMSD stabilization after the first 1 nanosecond. Consequently, the sampled trajectory used in the analyses reflects structures belonging to a more stable stage of the simulation, thus reducing artifacts because of differences between the periodic water box (MD) and the crystal environments (50,51). The RMSD comparison also illustrates that peptide **5** behaves similarly to the natural substrate TS_2. Both showed the same amount of deviations, whereas other peptides diverged slightly in RMSD values throughout the MD simulation.

The proteins compactness was also measured, calculating their gyration radius (Rg, Figure 2B), which revealed no significant conformational changes during the simulation. Taken together, these results (RMSD and Rg) assured that the simulations were reasonably stable and the data used for analysis are reliable.

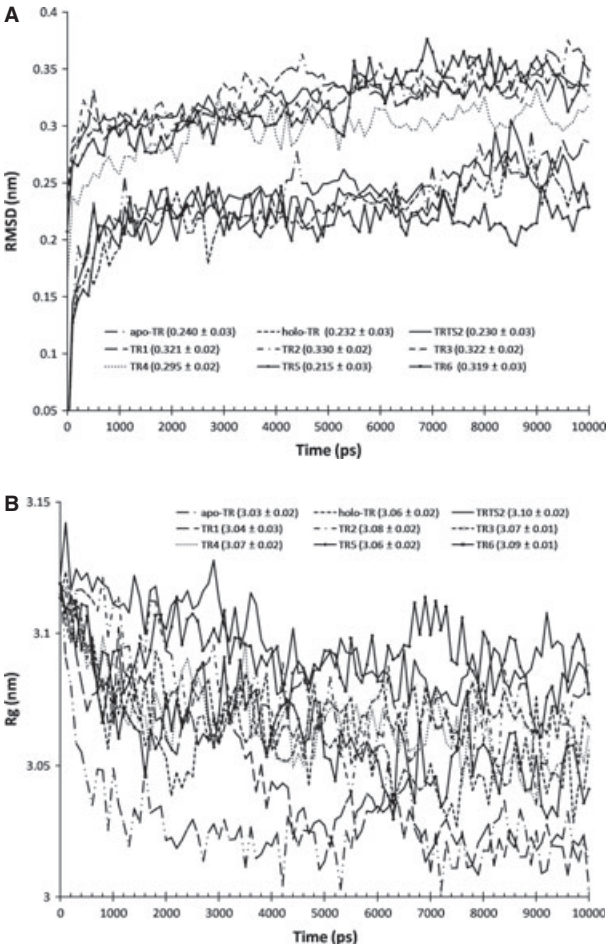

Figure 2: (A) Time evolution of the root-mean-square deviation (nm) calculated on protein atoms positions over the 10 nanoseconds molecular dynamics simulation with respect to their initial structures (after equilibration). The systems are coded as follows: *apo*-TR (free TR), *holo*-TR (TR + FAD), TRTS2 (TR + FAD + TS2), and TR1-6 (TR + FAD + peptide **1**–**6**) (see Table 1). (B) Time evolution of the radius of gyration (Rg, nm) for the TR protein atoms. The legends are the same to (A). FAD, flavin-adenine-dinucleotide; TR, trypanothione reductase.

Active site rigidity and substrate/inhibitor flexibility

The TR-substrate interactions have been termed 'mould-and-melt fit', i.e., the rigid active site presents a cavity (or mould) of defined shape, where the flexible (or molten) substrate binds via a correct orientation and conformation, pressured by non-covalent interactions (25). Moreover, studies in the TR–TS_2 complex revealed that the TS_2 binding mechanism was determined by the electronically 'induced-fit' process when the amino acid of the active center, $H^{461'}$, is itself activated by the substrate that will be further processed (27).

To evaluate these hypotheses, the atomic backbone TR residues fluctuations were calculated in all complexes, shown in Figure 3 as a 3-D representation. Figure 3 shows that the most potent TR inhibitors (**4**, **5** and **6**) presented fluctuations similar to the natural substrate, whereas the least potent inhibitors (**1** and **2**) destabilized the TR protein, mainly at the FAD and NADPH binding domains. In addition, the cyclic substrate is responsible for higher perturbation in enzyme than the peptides, which are more flexible to direct and to perform stronger interactions, not allowing many fluctuations in protein chains (Figure 3).

Influence of the SASA

The SASA calculation can increase the understanding about the hydrophobic influence in the TR peptide inhibition. The SASA was calculated by the DSSP program (52), which gives the maximal accessible surface of a residue considering its insertion in a glycine

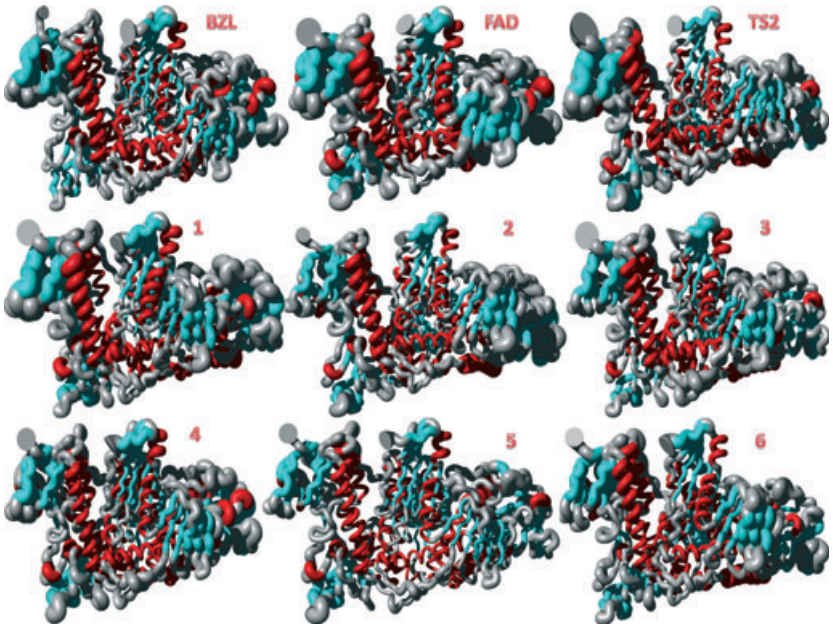

Figure 3: Three-dimensional graphical representation of the root mean square fluctuation (3-D root-mean-square deviation) calculated for trypanothione reductase backbone atoms over the 10 nanoseconds of simulation. Three regions should be mentioned that are present in all structures: active site domain (central cleft), flavin-adenine-dinucleotide binding domain (upper left loop), and NADPH binding domain (right bends). The figures were generated using MOLMOL program (52) and the legends are the same as Figure 2A. The secondary structures are colored as following: alpha-helices in red, beta-sheet in blue and unstructured regions in gray.

chain. The SASA subtraction for the ligand, bound or not to TR, results in the amount of contacts lost by the ligand when it interacts with the enzyme. These data are shown in Table 1 for each ligand.

Bailey *et al.* (25) asserted that approximately 66% of the N^1-glutathionyl spermidine disulfide area becomes buried when the enzyme-substrate complex is formed, which means that the binding hydrophobic component is around 84 kJ/mol. The authors concluded that the hydrophobic cleft in the active site plays an important role for stabilizing the complex (25). Bond *et al.* (27) calculated TS_2 SASA and the result of about 87% (850 $Å^2$, ~85 kJ/mol) in the lost area was in good agreement with the previous published data (25). Our SASA results for the natural substrate are also in agreement with the experimental data (25,27), as we achieved 81% for the area loss (Table 1).

The chemical diversity in the peptide inhibitors studied herein was reflected in their SASA values during the MD. However, it is not possible to use solely the 'absolute' SASA values to profile the peptide inhibitory. In the following cases we will show how we came to that conclusion.

First in peptides **1** and **2** (Table 1), slightly dissimilar results could reveal that these peptide lost when interacting with TR should be somewhat distinct, despite their identical sequence. The three BNF derivatives (**5**, **3** and **6**) have lost approximately 0.65% of their areas, justifying the coincident values found in our calculations. Compound **4** is the only one that augmented its area, possibly because of more favorable interaction with the aqueous media through PNO branches.

Hydrogen bonds analysis

The number of hydrogen bonds (Hbond) were first analyzed using the *g_hbond* module of GROMACS package (34). Table 1 shows the number of hydrogen bonds averaged over the 10 nanoseconds. The number of Hbond between the TR and the ligands was obtained calculating the existence, or not, of a hydrogen bond by following the geometric criteria: (i) cutoff distance between heavy atoms donor and acceptor of 3.5 Å and (ii) cutoff angle acceptor-donor-hydrogen of 60° (36).

From this analysis, we note that almost all peptide inhibitors (except derivative **2**) presented a higher number of Hbond than the natural substrate. Based on this information, we, then, classified the complexes in three different groups: (i) (5–6 Hbond), comprising TS_2 and peptide **2**; (ii) 6–7 Hbond, peptides **1**, **3** and **4**, and (iii) more than seven Hbond, for the tighter inhibitors (**5** and **6**). Pointing out that derivatives **5** and **6** have the equivalent activity, and **4** has approximately 100-times the activity of peptide **3** (Table 1), it is important to remind that analyzing only the numbers of Hbond could not reveal these peptides inhibitory behavior. Thus, we also discriminated against the protein residues that interact with our inhibitors and calculated permanency through the simulation. For permanency analysis, we chose a cutoff time of ≥10% durability, which means at least 1 nanosecond of stability in this interaction. These results are shown in Table 2.

Table 2: Time permanency of hydrogen bonds (Hbonds) formed between trypanothione reductase and the ligands atoms during the molecular dynamics simulation

Name	Time permanency (%)	Protein residue[a]	Ligand residue[b]
TS2	51.45	E19 OE2	*TS_2* NAT
	48.75	E19 OE1	*TS_2* NAT
	29.37	S110 OG	*TS_2* OBG
	89.81	Y111 OH	*TS_2* OAS
	30.57	Y111 OH	*TS_2* OAO
	17.08	H461′ NE2	*TS_2* NAJ
	11.39	E466′ OE2	*TS_2* NBN
1	92.81	E19 OE2	HISH1 ND1
	96	E19 OE1	HISH1 ND1
	20.18	E19 OE2	HISH1 N
	17.18	E19 OE1	HISH1 N
	50.75	E466′ OE2	HISH1 NE2
	53.55	E466′ OE1	HISH1 NE2
2	67.03	E19 OE2	HISH1 NE2
	63.84	E19 OE1	HISH2 NE2
	44.86	S110 OG	HISH1 N
3	54.15	E19 OE2	GLY2 N
	62.54	E19 OE1	GLY2 N
	39.06	E19 OE2	ARG3 N
	40.76	E19 OE1	ARG3 N
	23.48	Y111 OH	BNF6 N
	65.93	Y111 OH	BZO1 O
	38.46	E466′ OE1	ARG3 NE
	16.48	E466′ O	ARG3 NH1
	19.48	E466′ OE1	ARG4 NE
	12.39	E466′ OE2	ARG4 NH1
	45.65	C469′ O	ARG3 NH2
	45.75	C469′ O	ARG3 NH1
	12.19	S470′ OG	ARG4 NH2
4	53.25	E19 OE2	ARG2 NE
	44.26	E19 OE1	ARG2 NE
	15.28	E19 N	BEZ1 O
	35.86	E19 OE2	ARG2 NH2
	39.06	E19 OE1	ARG2 NH2
	10.09	Y111 OH	ARG2 N
	11.59	Y111 OH	BEZ1 O
	16.28	H461′ NE2	ARG2 NH1
	14.59	E466′ OE2	ARG3 NE
	27.07	E466′ OE1	ARG3 NH2
	20.18	E467′ OE1	ARG3 NE
	12.59	E467′ OE2	ARG3 NH1
	10.39	E467′ OE1	ARG3 NH1
	33.07	E467′ OE2	ARG3 NH2
	28.17	E467′ OE1	ARG3 NH2
	20.88	C469′ O	ARG2 NH2
	44.46	C469′ O	ARG2 NH1
	16.98	S470′ OG	ARG2 NH1
	18.48	R472′ NH2	ARG2 O
5	78.82	E19 OE1	ARG3 N
	23.78	Y111 OH	ARG4 NH2
	74.73	Y111 OH	BNF5 N
	38.46	H461′ NE2	ARG4 NE
	62.04	H461′ NE2	ARG4 NH1
	33.67	E466′ O	ARG3 NH1
	15.08	C469′ O	ARG3 NH2
	67.43	S470′ OG	ARG3 NE
	54.35	S470′ OG	ARG3 NH1
	36.66	R472′ NE	LEU2 O
	15.98	R472′ NH1	LEU2 O
	19.48	R472′ NH2	ARG4 O
	28.67	R472′ NH2	ARG3 O
	19.58	R472′ NH2	LEU2 O
6	36.46	E19 OE2	ALA2 N
	35.16	E19 OE1	ALA2 N
	30.27	E19 OE2	ARG3 N
	69.93	E19 OE1	ARG3 N
	53.95	E19 OE2	ARG4 N
	24.58	E19 OE1	ARG4 N
	73.33	Y111 OH	ARG3 NH2
	57.44	Y111 OH	ARG3 NH1
	17.78	R472′ NE	ALA2 O
	15.88	R472′ NE	BEZ1 O
	16.48	R472′ NH2	BEZ1 O

[a]The prime character (′) means that the residues belongs to chain B of the enzyme.
[b]The numbers after the ligands residues represent the part of the molecule discriminated at Table 1. The abbreviations used are the same from Table 1 (see Figure 1 for chemical structure details).

Several TR residues were pointed out by many authors as interacting with TS_2 (25–27,53,54). From our simulations, we should remark some of them: *E^{19}*, *S^{110}*, *Y^{111}*, and *$H^{461'}$*. The first hydrogen bond is related to glutamic acid (*E^{19}*), representing the interactions between SPM and peptide Gly-I (25,27) bond. This interaction was reproduced at our simulations for the natural substrate TS_2 (Table 2). We also noted that all inhibitors presented significant Hbond with this acidic residue (≥50% permanency time), which reinforces the linkage between enzyme at this region and strong inhibitors, as suggested by some authors (25–27).

Trypanothione (TS_2) has two Hbond with the *Y111*, which is according to the literature (27) strengthens our simulation data (Table 2). Except peptide **4** (∼11% of permanency) and lower potent inhibitors (**1**,**2**), which do not have this Hbond, all other derivatives interact through two different Hbond, with percentages higher than 24% and attended the activity potency.

Histidine 461′ was first described to interact with gamma sulfur in Cys-I of the N1-gluthathionyl spermidine (25), Zhang *et al.* (26) postulated that one water molecule could provide the proton charge for the histidine in catalysis, and Bond *et al.* (27) expanded this idea assuring one Hbond between *$H^{461'}$* and *gamma*-Glu-II of the substrate. This interaction was presented only by the natural substrate (TS_2) and peptides **5** and **4** (Table 2). However, when we analyzed the other *γ-glutamic site* residues formers, i.e., *$E^{466'}$* and *$E^{467'}$*, where the glutamic residues acts as 'Glu pincers' (53), we observed a strong interaction with both glutamic residues, higher than the substrate and not present in derivative **6**, for most potent inhibitors (**4**, **5**). The less potent inhibitors (**1**, **2** and **3**) presented higher Hbond values with these glutamic residues, but only these interactions are not crucial in inhibitory pattern (Table 2). As *γ-glutamic site* is very important in the discrimination of the inhibitor

behavior, the high values of interaction with this site will not indicate that we have a good in inhibitor.

S^{110} is conserved in all *Trypanosomatidae* species and can participate in a hydrogen bond with the substrate (26). Some authors made special remarks for this Hbond when related to SPM derivatives (25,26), and our calculations showed that we can reproduce this interaction with a significant percentage above 29% (Table 2). Our peptides have not interacted with this residue, except derivative **2**. However, we can note that other serine residue (*S470′*) resembles this hydrogen bond with the peptides. This interaction was not reported before, and because of its percentages we decided to describe it more precisely.

S470′ is located near the active site entrance and has two other Hbond-capable residues in this region: *C469′* and *R472′* (Figure 4). This site cannot be accessed by trypanothione, reminding the 'Z-site' (53) description. This part of enzyme was used to describe the specific TR inhibitors activity. Nowadays, it is well established in the drug design of TR inhibitors (53,54). The peptide inhibitors have Hbond with these three residues (*C469′* through its backbone atoms, *S470′*, *R472′*) in high permanency times (more than 15% durability). The deviations in this behavior were the lower potents **2** and **1**. These hydrogen bonds with elevated durability, with diverse peptide inhibitors, assure us our results reliance, indicating that this region could be a new site in TR for development of new inhibitors.

Mapping the contact areas

The SASA can be related to the hydrophobic contribution for binding as stated in refs (25,27). The DSSP analysis (52) revealed us the magnitude of the interactions loss when a ligand is bound to the TR. None was declared to detail the protein atoms contribution in the peptides inhibitor behavior. Some authors have indicated many residues important for interactions with higher inhibitors (22,24–27) and they have been explored in the development of the new lead compounds (16).

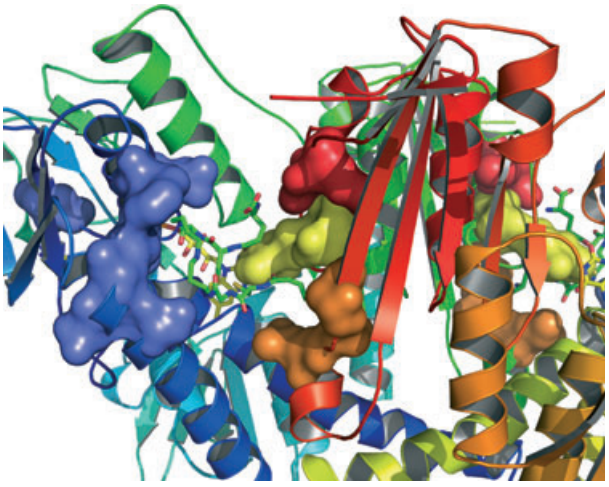

Figure 4: Schematic representation of trypanothione reductase showing the natural substrate (green sticks), flavin-adenine-dinucleotide (yellow sticks) and four sub-sites: hydrophobic cleft (blue surface), Z-*site* (orange surface), γ-glutamic site (yellow surface) and new interacting site (red surface). The figure was generated using PYMOL program (53).

We computed the individual contribution of each TR residue when interacting with the ligands, using a program developed in our lab, 'SURFINMD' software. It calculates the area in contact through a sphere probe of 1.4 nm and gave us the results through 10 nanosecond of simulation.

The high resolution crystallographic structure of TR obtained in 1999 (27) clarified some interactions involving the TR and their natural substrate. With an active site presenting 1.5 nm wide, 1.5 nm deep, and 2.0 nm in length, the enzyme has many residues to contact with the trypanothione disulfide (27) shown in Tables 3 and 4.

Evaluating TR peptides area that interface the ligands (Table 3) we first compared our results with the experimental one described before (27). The TS_2 could be schematically divided into their seven monomers (Glu-I, Cys-I, Gly-I, SPM, Gly-II, Cys-II, Glu-II, Figure 1), and the amino acids that contact with the substrate are the same as listed by Bond *et al.* (27): S^{15}, W^{22}, V^{54}, V^{59}, I^{107}, S^{110}, Y^{111}, T^{335}, I^{339}, $H^{461'}$, $P^{462'}$, $T^{463'}$, $S^{464'}$, $E^{466'}$, and $E^{467'}$. Our calculations revealed other residues in contact with trypanothione (TS_2), as will be explained later.

Sub-sites of TR active site

Chan *et al.* (53) described phenothiazine inhibitors into the trypanothione reductase active site and detached it in four minor sites (Figure 4): glutamic 19-site, γ-*glutamic* site (composed for $H^{461'}$, $E^{466'}$ and $E^{467'}$), the 'hydrophobic cleft' (L^{18}, W^{22}, Y^{111}, F^{112}, M^{114}) and 'Z-site' ($F^{396'}$, $P^{398'}$, and $L^{399'}$). As these protein parts presented diverse interactions, we detached each one at the following sections.

Glutamic 19-site

The side chains of E^{19} (former of the homonym site) and Y^{111} are responsible for hydrogen bonds with the peptide link between Gly-I and the substrate SPM (27). Our results in Tables 3 and 4 showed that all peptides have these interactions, which strengthen these significant contact interactions in our inhibitors.

γ-glutamic site

γ-*glutamic* site (Figure 4) was firstly described to justify the contact among inhibitors that contained quaternary nitrogen in phenothiazine inhibitors through glutamic residues presented there (53). After that, Khan *et al.* (54) studied the quaternary alkyl ammonium derivatives (stronger inhibitors than phenothiazine) intending to lodge their inhibitors positive charge. This enzyme region has the active-site proton donor and acceptor residues, the catalytic residue $H^{461'}$, where the imidazole is held in place with a hydrogen bond formed between $N^{\delta 1}$ and $O^{\varepsilon 1}$ of $E^{466'}$ (27). The last residue in γ-*glutamic* site is *E467′*, which is related to neutralizing at the active site, the positively substrates utilized by TR (25), as described in the catalysis mechanism proposed by (25).

Table 3: Area (Å^2) of the trypanothione reductase residues that interacts with ligands studied over the 10 nanoseconds molecular dynamics simulation

Site	Residue[a]	TS_2	**1**	**2**	**3**	**4**	**5**	**6**
E19 site	E19	14.69 ± 2.99	17.29 ± 4.45	8.86 ± 4.04	24.62 ± 7.27	21.02 ± 4.86	33.18 ± 6.67	22.87 ± 3.57
Hydrophobic cleft	L18	–	4.01 ± 4.56	1.62 ± 3.25	11.86 ± 6.11	9.14 ± 5.07	14.63 ± 6.55	–
	W22	8.39 ± 2.77	17.28 ± 9.36	21.51 ± 6.70	26.84 ± 10.72	16.89 ± 6.06	26.78 ± 5.55	20.16 ± 3.90
	Y111	24.69 ± 4.55	10.1 ± 7.03	12.37 ± 10.98	36.84 ± 17.93	25.15 ± 6.40	48.24 ± 8.46	21.83 ± 3.89
	M114	8.71 ± 2.78	21.12 ± 4.26	29.90 ± 4.95	25.24 ± 10.49	7.84 ± 25.23	32.06 ± 5.60	27.58 ± 5.90
Z-site	F396′	24.09 ± 5.99	3.35 ± 2.86	–	15.76 ± 4.63	8.65 ± 2.88	–	9.02 ± 11.09
	P398′	8.25 ± 3.81	6.83 ± 3.95	–	17.7 ± 4.46	11.33 ± 4.07	–	–
	L399′	24.68 ± 4.25	1.70 ± 2.43	2.85 ± 5.34	6.24 ± 5.73	9.99 ± 3.51	–	3.88 ± 5.67
γ-Glu site	H461′	16.78 ± 5.01	3.35 ± 2.86	–	15.76 ± 4.63	8.65 ± 2.88	–	4.16 ± 4.26
	E466′	17.67 ± 6.50	6.83 ± 3.95	–	17.69 ± 4.46	11.33 ± 4.06	–	7.47 ± 5.86
	E467′	21.70 ± 6.09	1.70 ± 2.43	2.85 ± 5.34	6.24 ± 5.73	9.99 ± 3.51	–	16.12 ± 10.46
New interacting site	C469′	–	–	–	6.43 ± 3.85	8.81 ± 4.44	–	2.85 ± 3.06
	S470′	2.79 ± 2.42	7.87 ± 4.14	3.11 ± 5.53	12.91 ± 5.13	12.5 ± 4.36	–	13.27 ± 9.15
	M471′	–	1.81 ± 4.48	–	–	–	–	1.03 ± 1.39
	R472′	–	36.79 ± 10.92	–	–	24.73 ± 10.03	–	29.77 ± 4.36

The area was calculated by 'SURFINMD' software representing the contact between ligands and trypanothione reductase residues (mean ± SD).
[a]The prime character (′) means that the residues belongs to chain B of the enzyme.

In Table 3, we note that all three residues reach the TS_2 closely. That is expected because contacts with catalytic residues should be optimized when the enzyme fits the natural substrate (26,27) and it was noted at our contacts results (Table 3).

For the most active peptides (**6**, **5** and **4**), we can realize that the contacts are higher when compared with the least potent compounds (**1**, **2** and **3**), where some interactions did not exist (Table 3). Another conclusion from *γ-glutamic* site contacts is its *charge complementarity* (26), to be further discussed. At this moment, we hint that derivative **2** (neutral molecular charge, Table 1) presented no interactions higher than 0.3 nm within the *γ-glutamic* site (Table 3), whereas the highly charged peptides – **5**, **6**, and **4** (Table 1) interact tightly with the charged amino acids (Table 3).

Hydrophobic cleft

Bailey *et al.* described the *C. fasciculata* TR that SPM chain fits into a hydrophobic niche formed at the residues W^{21} and M^{113} (25) site. They pointed out that M^{113} partakes in van der Waals interactions with the substrate, and W^{21} stacks over the SPM segment, helping to produce the most contacts between enzyme and substrate in one corner of the active site (25).

Zhang *et al.* (26) assure that hydrophobic patch serve to bind the aliphatic substrate moiety and that its '*charge complementarity*' is not limited to the active site, but extends out and around the clefts (26). They also indicated that the flexibility of the W^{22} side chain should be appending the inhibitor design together with the van der Waals contacts between I^{107}, Y^{111}, and TS_2. Using this information, Chan *et al.* anchored the phenothiazine inhibitors at this hydrophobic site and signaled this region as the accessible hydrophobic region (53). The high-resolution TR crystal revealed that: the hydrophobic site is adjacent to *γ-glutamic* site, and, there is a cation-π interaction between the hydrophobic patch and the substrate (27). Again, the methionine residue appears as an important residue contributing to the hydrophobic patch on one side of the active site (27).

From our contact results for the hydrophobic cleft, only L^{18} (Table 3) interacts with the hydrophobic patch in the SPM chains (27), with no significant contact area with the substrate. This could be because of the nature of the 'crystallographic' contact when Gly-I (Figure 1), porting a hydrogen sidechain, interacts with this residue. Except for peptide **3** (bulkier peptide), all derivatives reproduce this contact comparable with their activity values (pI_{50}, Table 1).

W^{22} is claimed to interact through hydrophobic contacts with SPM bridge of the natural substrate (25–27), which was very well reproduced in our simulations (Table 3). The contacts between W^{22} and the peptide inhibitors emphasized this relevant residue in this site.

M^{114} has been seen interacting with TS_2, as another main hydrophobic contribution (25–27,53,54). Table 3 shows that all peptides presented higher contacts with the M^{114} than W^{22}, which could support the particular relevancy of this methionine, because of its aforementioned characteristics when interacting with the peptide inhibitors.

However, the highest contacts value in this site is because of Y^{111}. This residue could interact through hydrogen bonds (as stated before), and in an aromatic manner with SPM bridge (27). The overall contacts succeeded the pI_{50} order, except for **1**, **2,** and **6** derivatives. Tyrosine sidechain interactions can be didactically divided into two parts: Hbond interactions, and the contact surface area. Analyzing the Y^{111} contacts, we noted few contacts for peptide **6** (Table 3), which could suggest that this interaction is not important in this potent derivative inhibition mechanism – the same thought could be applied to a reverse mode to derivative **3**. Although remarking the Hbond data, compound **6** is tightly bound to the enzyme through Y^{111} in more than 50% of simulation time (Table 2),

Table 4: Area (Å^2) of the each ligand that interacts with trypanothione reductase residues studied over the 10 nanoseconds molecular dynamics simulation

Ligands[a]	Contact area[b]
TS_2	
γ Glu-Cys-Gly I	132.50 ± 12.81
SPM	57.3 ± 7.2
γ Glu-Cys-Gly II	127.32 ± 9.18
1	
HIS	68.37 ± 8.52
TRP	69.95 ± 8.99
LYS	37.15 ± 14.71
2	
HIS	55.32 ± 5.99
TRP	64.50 ± 12.40
HIS	47.39 ± 10.93
3	
BZO	54.91 ± 7.76
GLY	28.00 ± 4.53
ARG	82.92 ± 9.01
ARG	26.99 ± 20.13
LEU	34.46 ± 9.99
BNF	41.46 ± 25.99
4	
BEZ	63.94 ± 7.14
ARG	78.61 ± 12.14
ARG	61.04 ± 11.54
PNO	54.43 ± 6.43
5	
BZO	39.68 ± 7.71
LEU	44.49 ± 6.68
ARG	21.62 ± 4.05
ARG	56.72 ± 5.47
BNF	58.75 ± 8.59
6	
BEZ	76.97 ± 6.93
ALA	27.04 ± 6.41
ARG	53.63 ± 9.52
ARG	70.37 ± 5.89
BNA	50.25 ± 9.84

BEZ, benzyloxycarbonyl; BNF, β-naphtylamide; BZO, benzoyl; PNO, para-nitroanilide; SPM, spermidine.

[a]Group Name of each ligand defined as shown at Figure 1.

[b]Contact area was calculated by SURFINMD program v. 1.05. This numbers represents the area between ligands and trypanothione reductase (mean ± SD).

which confirms its convincing activity and could apparently be contradictory, when analyzing just the tyrosine surface area. Taken together, the Hbond and contact area support the importance of evaluating the inhibitory behavior with multiple tools to ensure the reliability of the results.

'Z-site'

Chan *et al.* described some residues, $F^{396'}$, $P^{398'}$, and $L^{399'}$, forming the second hydrophobic pocket at TR, not accessed by substrate trypanothione (53). This site was called 'Z-site' (Figure 4), and at our contact calculations, we cannot assign these residue contributions for the peptides inhibitory activity (data not shown).

New interacting residues

Based on our MD analysis we were able to describe some new interacting residues not described before by any author. These residues presented significant contacts with the peptide inhibitors: $C^{469'}$, $S^{470'}$, and $R^{472'}$ (Figure 4). The electrostatic behavior through Hbond was explained before in its specific topic. The serine residue, which was postulated to resemble the S^{110} Hbond, made some non-polar contacts with inhibitors, following the activity order (Table 3). Another residue, $R^{472'}$, have similar results for contacts with the peptides. These contacts with the hydrogen bonds analysis results should lead the accessibility of this site for future most potent inhibitors.

Conclusions

Mc Kie *et al.* synthesized a series of peptide mimetics that inhibited the *T. cruzi* TR (22). In the present work, we intended to understand these compounds dynamic inhibitory behavior when bound to this enzyme, applying MD simulations. The six complexes were built in a dodecahedral box containing: protein, peptide inhibitor, SPC water, and counter-ions, giving an amount of 139 000 atoms.

Overall, the TR adopts a particular conformation when facing these inhibitors, depending on their potency. The peptides have higher freedom degrees than the SPM substrate, and presented more contacts with TR residues than the substrate (TS_2), which is regarded as efficient inhibitors in tightly binding mode in their targets. These contacts represent some diverse interactions, e.g., hydrogen bonds and surface contacts, represented by hydrophobic and van der Waals counterparts.

Using MD and multiple analysis tools, we reproduced the experimental inhibitory data reports by Mc Kie *et al.* (24) and reported the main sites related to this behavior, e.g., glutamic 19-site, *γ-glutamic* site (composed for $H^{461'}$, $E^{466'}$ and $E^{467'}$), the 'hydrophobic cleft' (L^{18}, W^{22}, Y^{111}, F^{112}, M^{114}), and 'Z-site' ($F^{396'}$, $P^{398'}$ and $L^{399'}$). Based on our present results, we should affirm that any particular analysis (Hbond pattern, 3-D RMSD, SASA, etc.) cannot be used apart from the others to justify the main interaction between TR residues and peptide inhibitors.

Moreover, we describe other residues in TR that can be accessed in the aperture of the enzyme: $C^{469'}$, $S^{470'}$, $M^{471'}$, $R^{472'}$. At this point, we judged this region interesting for the development of new powerful inhibitors against TR, but new insights could be obtained using useful MD models that might reveal other affordable regions to explore, even more diverse than that reported here.

Acknowledgments

Samuel Pita thanks Dr. K. Anton Feenstra for kindly gifting the FAD parameters for GROMOS96 Force Field. All authors are grateful to the Brazilian agencies (CNPq, CAPES and FAPERJ) for financial support and to the Instituto de Biofísica Carlos Chagas Filho (IBCCF-UFRJ) for computational facilities.

References

1. Chagas C. (1909) Nova tripanosomiaze humana. Mem Inst Oswaldo Cruz;1:11–80.
2. Jannin J., Villa L. (2007) An overview of Chagas disease treatment. Mem Inst Oswaldo Cruz;102(Suppl. 1):95–97.
3. Jackson Y., Myers C., Diana A., Marti H.P., Wolff H., Chappuis F. *et al.* (2009) Congenital transmission of chagas disease in Latin American immigrants in Switzerland. Emerg Infect Dis;15:601–603.
4. Lescure F.X., Canestri A., Melliez H., Jaureguiberry S., Develoux M., Dorent R. *et al.* (2008) Chagas disease, France. Emerg Infect Dis;14:644–646.
5. Salinas A.D.G.M., Fernández-Guerrero M. (2007) Chagas' disease: a growing problem in Spain. Chagas' Disease: A Growing Problem in Spain. 17th European Congress of Clinical Microbiology and Infectious Diseases: European Society of Clinical Microbiology and Infectous Disease.
6. Milei J., Guerri-Guttenberg R.A., Grana D.R., Storino R. (2009) Prognostic impact of Chagas disease in the United States. Am Heart J;157:22–29.
7. de-Ayala A.P., Perez-Molina J.A., Norman F., Lopez-Velez R. (2009) Chagasic cardiomyopathy in immigrants from Latin America to Spain. Emerg Infect Dis;15:607–608.
8. Schmunis G.A. (2007) Epidemiology of Chagas disease in non-endemic countries: the role of international migration. Mem Inst Oswaldo Cruz;102(Suppl. 1):75–85.
9. Hotez P.J., Molyneux D.H., Fenwick A., Kumaresan J., Sachs S.E., Sachs J.D. *et al.* (2007) Control of neglected tropical diseases. N Engl J Med;357:1018–1027.
10. Krauth-Siegel R.L., Comini M.A. (2008) Redox control in trypanosomatids, parasitic protozoa with trypanothione-based thiol metabolism. Biochim Biophys Acta;1780:1236–1248.
11. Junnila J.L. (2010) Chagas disease as secondary cause of cardiomyopathy. Am Fam Physician;81:407.
12. Urbina J.A. (2001) Specific treatment of Chagas disease: current status and new developments. Curr Opin Infect Dis;14:733–741.
13. Dias J.C., Silveira A.C., Schofield C.J. (2002) The impact of Chagas disease control in Latin America: a review. Mem Inst Oswaldo Cruz;97:603–612.
14. Cunha E.F.F.R.T., Mancini D.T., Fonseca E.M.B., Oliveira A.A. (2010) New approaches to the development of anti-protozoan drug candidates: a review of patents. J Braz Chem Soc;21:1787–1806.
15. Fairlamb A.H., Blackburn P., Ulrich P., Chait B.T., Cerami A. (1985) Trypanothione: a novel bis(glutathionyl)spermidine cofactor for glutathione reductase in trypanosomatids. Science;227:1485–1487.
16. Krauth-Siegel R.L., Inhoff O. (2003) Parasite-specific trypanothione reductase as a drug target molecule. Parasitol Res;90(Suppl. 2):S77–S85.
17. Allaoui A., Francois C., Zemzoumi K., Guilvard E., Ouaissi A. (1999) Intracellular growth and metacyclogenesis defects in *Trypanosoma cruzi* carrying a targeted deletion of a Tc52 protein-encoding allele. Mol Microbiol;32:1273–1286.
18. Dumas C., Ouellette M., Tovar J., Cunningham M.L., Fairlamb A.H., Tamar S. *et al.* (1997) Disruption of the trypanothione reductase gene of *Leishmania* decreases its ability to survive oxidative stress in macrophages. EMBO J;16:2590–2598.
19. Kelly J.M., Taylor M.C., Smith K., Hunter K.J., Fairlamb A.H. (1993) Phenotype of recombinant *Leishmania donovani* and *Trypanosoma cruzi* which over-express trypanothione reductase. Sensitivity towards agents that are thought to induce oxidative stress. Eur J Biochem;218:29–37.
20. Krieger S., Schwarz W., Ariyanayagam M.R., Fairlamb A.H., Krauth-Siegel R.L., Clayton C. (2000) Trypanosomes lacking trypanothione reductase are avirulent and show increased sensitivity to oxidative stress. Mol Microbiol;35:542–552.
21. Maccari G., Jaeger T., Moraca F., Biava M., Flohe L., Botta M. (2011) A fast virtual screening approach to identify structurally diverse inhibitors of trypanothione reductase. Bioorg Med Chem Lett;21:5255–5258.
22. Benson T.J., McKie J.H., Garforth J., Borges A., Fairlamb A.H., Douglas K.T. (1992) Rationally designed selective inhibitors of trypanothione reductase. Phenothiazines and related tricyclics as lead structures. Biochem J;286(Pt 1):9–11.
23. Schirmer R.H., Muller J.G., Krauthsiegel R.L. (1995) Disulfide-reductase inhibitors as chemotherapeutic-agents – the design of drugs for trypanosomiasis and malaria. Angew Chem Int Ed Engl;34:141–154.
24. McKie J.H., Garforth J., Jaouhari R., Chan C., Yin H., Besheya T. *et al.* (2001) Specific peptide inhibitors of trypanothione reductase with backbone structures unrelated to that of substrate: potential rational drug design lead frameworks. Amino Acids;20:145–153.
25. Bailey S., Smith K., Fairlamb A.H., Hunter W.N. (1993) Substrate interactions between trypanothione reductase and N1-glutathionylspermidine disulphide at 0.28-nm resolution. Eur J Biochem;213:67–75.
26. Zhang Y., Bond C.S., Bailey S., Cunningham M.L., Fairlamb A.H., Hunter W.N. (1996) The crystal structure of trypanothione reductase from the human pathogen *Trypanosoma cruzi* at 2.3 A resolution. Protein Sci;5:52–61.
27. Bond C.S., Zhang Y., Berriman M., Cunningham M.L., Fairlamb A.H., Hunter W.N. (1999) Crystal structure of *Trypanosoma cruzi* trypanothione reductase in complex with trypanothione, and the structure-based discovery of new natural product inhibitors. Structure;7:81–89.
28. Leichus B.N., Bradley M., Nadeau K., Walsh C.T., Blanchard J.S. (1992) Kinetic isotope effect analysis of the reaction catalyzed by *Trypanosoma congolense* trypanothione reductase. Biochemistry;31:6414–6420.
29. van den Berg P.A.W., Feenstra K.A., Mark A.E., Berendsen H.J.C., Visser A.J.W.G. (2002) Dynamic conformations of flavin adenine dinucleotide: simulated molecular dynamics of the flavin cofactor related to the time-resolved fluorescence characteristics. J Phys Chem B;106:8858–8869.
30. Iribarne F., Paulino M., Aguilera S., Tapia O. (2009) Assaying phenothiazine derivatives as trypanothione reductase and glutathione reductase inhibitors by theoretical docking and Molecular Dynamics studies. J Mol Graph Model;28:371–381.
31. Berman H.M., Westbrook J., Feng Z., Gilliland G., Bhat T.N., Weissig H. *et al.* (2000) The Protein Data Bank. Nucleic Acids Res;28:235–242.

32. da Rocha Pita S.S., Cirino J.J., de Alencastro R.B., Castro H.C., Rodrigues C.R., Albuquerque M.G. (2009) Molecular docking of a series of peptidomimetics in the trypanothione binding site of *T. cruzi* trypanothione reductase. J Mol Graph Model;28:330–335.
33. Guex N., Peitsch M.C. (1997) SWISS-MODEL and the Swiss-PdbViewer: an environment for comparative protein modeling. Electrophoresis;18:2714–2723.
34. Lindahl E., Hess B., van der Spoel D. (2001) GROMACS 3.0: a package for molecular simulation and trajectory analysis. J Mol Model;7:306–317.
35. Van der Spoel D., Lindahl E., Hess B., Groenhof G., Mark A.E., Berendsen H.J.C. (2005) GROMACS: fast, flexible, and free. J Comput Chem;26:1701–1718.
36. van der Spoel D., Lindahl E., Hess B., van Buuren A.R., Apol E., Meleunhoff P.J. *et al.* (2005) Gromacs User Manual Version 3.3. p. 83–109.
37. Berendsen H.J.C., Postma J.P.M., Gunsteren W.F.V., Hermans J. (1981) Interaction models for water in relation to protein hydration. In: Pullman B., editor. Interaction Models for Water in Relation to Protein Hydration. Dordrecht: D. Reidel Publishing Company; p. 331–342.
38. Berk H., Henk B., Herman J.C.B., Johannes G.E.M.F. (1997) LINCS: a linear constraint solver for molecular simulations. J Comput Chem;18:1463–1472.
39. Miyamoto S., Kollman P.A. (1992) Settle – an analytical version of the shake and rattle algorithm for rigid water models. J Comput Chem;13:952–962.
40. Darden T., York D., Pedersen L. (1993) Particle mesh Ewald: an N·log(N) method for Ewald sums in large systems. J Chem Phys;98:10089–10092.
41. Berendsen H.J.C., Postma J.P.M., Vangunsteren W.F., Dinola A., Haak J.R. (1984) Molecular-dynamics with coupling to an external bath. J Chem Phys;81:3684–3690.
42. Connolly M.L. (1983) Solvent-accessible surfaces of proteins and nucleic-acids. Science;221:709–713.
43. Costa M., Batista P., Shida C., Robert C., Bisch P., Pascutti P. (2010) How does heparin prevent the pH inactivation of cathepsin B? Allosteric mechanism elucidated by docking and molecular dynamics BMC Genomics;11:S5.
44. Soares R.O., Batista P.R., Costa M.G.S., Dardenne L.E., Pascutti P.G., Soares M.A. (2010) Understanding the HIV-1 protease nelfinavir resistance mutation D30N in subtypes B and C through molecular dynamics simulations. J Mol Graph Model;29:137–147.
45. da Silva M.L., Goncalves A.D., Batista P.R., Figueroa-Villar J.D., Pascutti P.G., Franca T.C.C. (2010) Design, docking studies and molecular dynamics of new potential selective inhibitors of *Plasmodium falciparum* serine hydroxymethyltransferase. Mol Simulat;36:5–14.
46. Valiente P.A., Batista P.R., Pupo A., Pons T., Valencia A., Pascutti P.G. (2008) Predicting functional residues in *Plasmodium falciparum* plasmepsins by combining sequence and structural analysis with molecular dynamics simulations. Proteins;73:440–457.
47. Batista P.R., Wilter A., Durham E.H.A.B., Pascutti P.G. (2006) Molecular dynamics simulations applied to the study of subtypes of HIV-1 protease common to Brazil, Africa, and Asia. Cell Biochem Biophys;44:395–404.
48. Liwo A., Czaplewski C., Oldziej S., Scheraga H.A. (2008) Computational techniques for efficient conformational sampling of proteins. Curr Opin Struct Biol;18:134–139.
49. Bahar I., Lezon T.R., Bakan A., Shrivastava I.H. (2010) Normal mode analysis of biomolecular structures: functional mechanisms of membrane proteins. Chem Rev;110:1463–1497.
50. Janin J., Rodier F. (1995) Protein-protein interaction at crystal contacts. Proteins;23:580–587.
51. Batista P.R., Robert C.H., Marechal J.D., Ben Hamida-Rebai M., Pascutti P.G., Bisch P.M. *et al.* (2010) Consensus modes, a robust description of protein collective motions from multiple-minima normal mode analysis-application to the HIV-1 protease. Phys Chem Chem Phys;12:2850–2859.
52. Kabsch W., Sander C. (1983) Dictionary of protein secondary structure – pattern-recognition of hydrogen-bonded and geometrical features. Biopolymers;22:2577–2637.
53. Chan C., Yin H., Garforth J., McKie J.H., Jaouhari R., Speers P. *et al.* (1998) Phenothiazine inhibitors of trypanothione reductase as potential antitrypanosomal and antileishmanial drugs. J Med Chem;41:148–156.
54. Khan M.O., Austin S.E., Chan C., Yin H., Marks D., Vaghjiani S.N. *et al.* (2000) Use of an additional hydrophobic binding site, the Z site, in the rational drug design of a new class of stronger trypanothione reductase inhibitor, quaternary alkylammonium phenothiazines. J Med Chem;43:3148–3156.

Note

[a]SYBYL, 2004, USA: Typos Inc.